Estimation of rate constants in nonlinear reactions involving chemical inactivation of oxidation catalysts

Maria Emelianenko, Diego Torrejon, Matthew A. DeNardo, Annika K. Socolofsky, Alexander D. Ryabov & Terrence J. Collins

Journal of Mathematical Chemistry

ISSN 0259-9791

J Math Chem
DOI 10.1007/s10910-014-0322-4

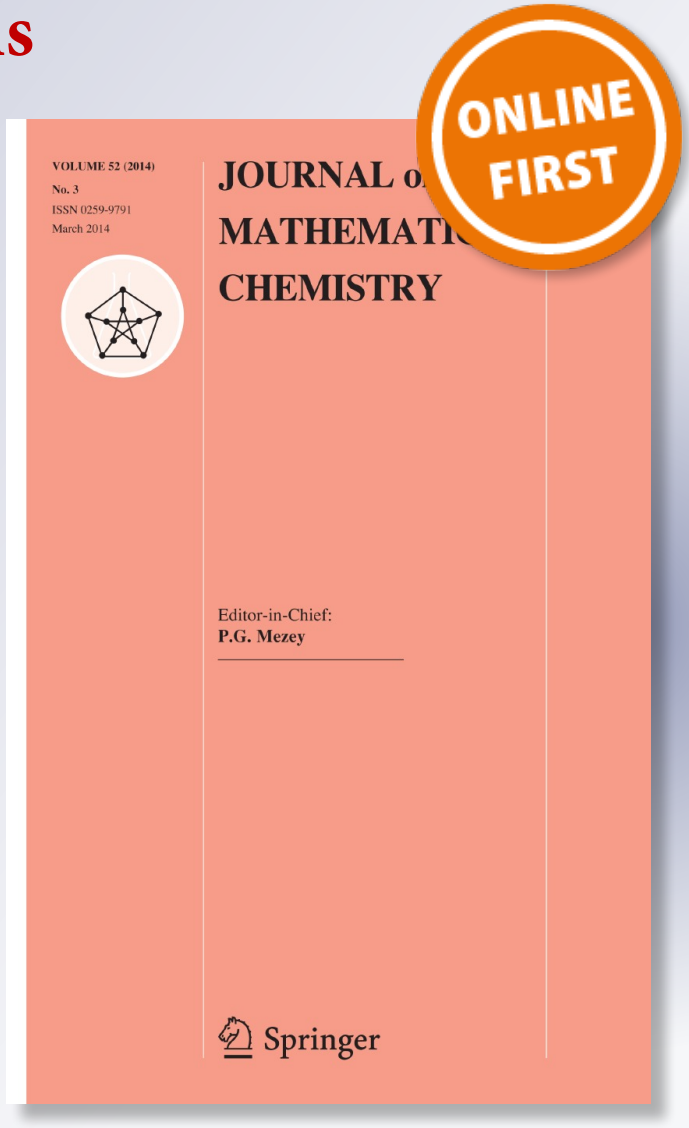

Springer

J Math Chem
DOI 10.1007/s10910-014-0322-4

ORIGINAL PAPER

Estimation of rate constants in nonlinear reactions involving chemical inactivation of oxidation catalysts

Maria Emelianenko · Diego Torrejon · Matthew A. DeNardo · Annika K. Socolofsky · Alexander D. Ryabov · Terrence J. Collins

Received: 20 November 2013 / Accepted: 28 January 2014

Abstract Over the last decades, copious work has been devoted to the development of small molecule replicas of the peroxidase enzymes that activate hydrogen peroxide in metabolic and detoxifying processes. TAML activators that are the subject of this study are the first full functional, small molecule peroxidase mimics. As an important feature of the catalytic cycle, TAML reactive intermediates (active catalysts, Ac) undergo suicidal inactivation, compromising the functional catalysis. Herein the relationship between suicidal inactivation and productive catalysis is rigorously addressed mathematically and chemically. We focus on a generalized catalytic cycle in which the TAML inactivation step is delineated by its rate constant k_{i} where the revealing data is collected in the regime of incomplete conversion of substrate (S) artificially imposed by the use of very low catalyst concentrations.

$$\begin{cases} \text{Resting catalyst (Rc)} + \text{Oxidant} \rightarrow \text{Ac} & (k_{\mathrm{I}}) \\ \text{Ac} + \text{Substrate (S)} \rightarrow \text{Rc} + \text{Product} & (k_{\mathrm{II}}) \\ \text{Ac} \rightarrow \text{Inactive catalyst} & (k_{\mathrm{i}}) \end{cases}$$

The system exhibits a nonlinear conservation law and is modeled via a singular perturbation approach, which is used to obtain closed form relationships between system parameters. A new method is derived that allows to compute all the rate constants in the catalytic cycle, k_{I}, k_{II}, and k_{i}, with as little as two linear least squares fits, for the

M. Emelianenko (✉) · D. Torrejon
Department of Mathematical Sciences, George Mason University,
4400 University Dr, Fairfax, VA 22030, USA
e-mail: memelian@gmu.edu

M. A. DeNardo · A. K. Socolofsky · A. D. Ryabov (✉) · T. J. Collins
Department of Chemistry, Carnegie Mellon University,
4400 Fifth Ave, Pittsburgh, PA 15213, USA
e-mail: ryabov@andrew.cmu.edu

Published online: 26 February 2014

minimal data set collected under any conditions providing that the oxidation of S is incomplete. This method facilitates determination of k_i, a critical rate constant that describes the operational lifetime of the catalyst, and greatly reduces the experimental work required to obtain the important rate constants.The approach was applied to the behavior of a new TAML activator, the synthesis and characterization of which are also described.

Keywords Iron TAMLs · Hydrogen peroxide · Catalyst inactivation · Ordinary differential equations · Mathematical modeling · Perturbation methods

1 Introduction

For many decades, chemists have been working to create low molecular weight homogeneous catalysts that can compete functionally with nature's ubiquitous oxidizing enzymes. The peroxidase enzymes that activate hydrogen peroxide to perform a myriad of biological oxidation processes are examples in point [1]. In a peroxidase enzyme nature embeds the prosthetic group, an iron-porphyrin complex, within a polypeptide framework. The polypeptide contributes what may be regarded as a series of design elements for marshaling enzymatic reactivity [2]. It adds to the propitious properties of the prosthetic group to facilitate the formation of potently oxidizing iron-oxo reactive intermediates and inhibits the facile suicide oxidative destruction of the porphyrin prosthetic groups.

Since small molecule replicas of these intricate enzymes are by definition not attired in large polypeptide coatings, alternative design strategies must be developed to find ways to minimize suicidal inactivation. We have approached this challenge systematically through the iterative design of ligand complements with an intrinsic resistance toward oxidative decomposition to advance far beyond the resistance typical of iron porphyrins. The decades-long enigma of whether or not and how this might be solved has been resolved with our development of TAML activators, which are complexes, especially iron complexes of tetraamido macrocyclic ligands **1** (Scheme 1) [3]. Iron(III) TAML activators deliver both oxidizing reactive intermediates that mimic the reactive entities in peroxidase catalysis and built-in resistance to suicide processes in what is basically a highly designed, but very simple structural motif [4]. However, there has been a real need for a method that is fast and straightforward for characterizing the catalytic performance of TAML activators under the operating conditions including the kinetic characterization of catalyst lifetimes. Therefore in this contribution, we describe a general approach for obtaining quantitative kinetic information relevant to TAML activator oxidation catalysis in solution. We have developed a universal method based upon both mathematics and chemistry that utilizes easily gathered experimental data to quantify the rate constant of catalyst decomposition under any operating conditions in addition to other key rate constants of the catalytic cycle.

Mathematically, the method is based on the singular perturbation theory that allows to separate the "slow" and "fast" dynamics of the stiff system of differential equations. The equation associated with the "slow" variable corresponds to the well-studied Quasi-Steady-State Approximation (QSSA) [5], while the other variable allows to

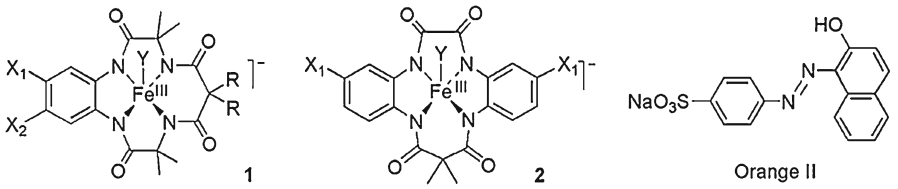

Scheme 1 First (**1**) and second (**2**) generations of Fe-TAML activators. Axial Y ligand is usually water or chloride. Catalyst **2** with $X_1 = CN$ and Orange II dye were used in this work

capture the rapid evolution of the system in the boundary layer. This approach has been applied to chemical kinetics problems by several authors [6,7], although none of the previous work has addressed the inherently nonlinear chemical inactivation problem. The main contribution of the present work is the derivation of a general mechanism for estimating rate constants based on the closed form representation of the solution obtained via the singular perturbation method. The method allows to obtain the full set of rate constants associated with the nonlinear kinetic model of chemical inactivation using only two linear least square fitting procedures. This approach is drastically different from the multiple variable optimization method sometimes called "kinetic modeling", which feeds a solution obtained by a full-blown stiff solver into a multi-parameter least squares optimization routine [8,9]. Given the nonlinear nature of the chemical inactivation problem described above, such a procedure would be costly, while yielding multiple plausible solution vectors indistinguishable from the point of view of the goodness of fit. In what follows, we develop a simple-to-use strategy that is devoid of these deficiencies while having a solid mathematical foundation.

2 Background and motivation

2.1 Background

Although TAML activators are potent oxidation catalysts, multiple degradation processes are known to bear directly on the catalytic performance in water (Scheme 2) [10]. A particular advantage of the method elaborated herein is that it provides a simple tool for evaluating the rate constant of the dominating degradation step. For catalyst design purposes, it is important to be able to rank the destructive capacity of each identified process by finding the intrinsic rate constants under operating conditions. Several decomposition pathways open up simply when TAML activators are dissolved in water. Thus, in the absence of an oxidizing agent the resting catalyst (Rc) decays due to demetalation (k_d) [11,12]. Still others come into play when hydrogen peroxide (H_2O_2) is added [13]. Upon peroxide addition, the Rc reacts reversibly (k_I, k_{-I}) with H_2O_2 to form the active catalyst (Ac), which then may attack the targeted substrate S in a product-producing reaction quantified by k_{II}. The intrinsic rate constants of the resting state demetalations are known to be immensely smaller than those associated with k_I and k_{II}, such that the former are of negligible significance under operating catalysis, but once the Ac has been formed, suicidal decomposition

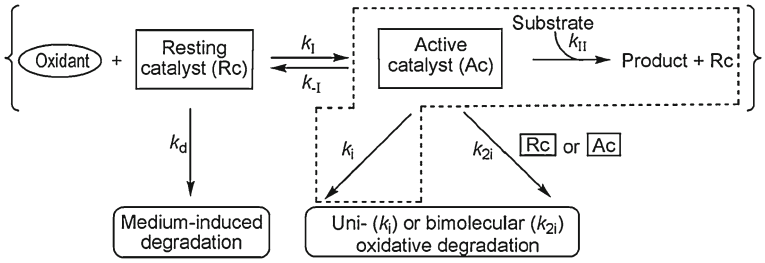

Scheme 2 General reaction scheme showing major catalytic steps and steps leading to inactivation of the resting state and the active form of an oxidation catalyst involved in a two-substrate process. A *dashed box* indicates a limited case analyzed in a previous work [13]

intrudes because the TAML ligand systems succumb slowly to the potent oxidizing properties of Ac [13].

There are at least two types of oxidative decomposition processes in TAML catalysis. Firstly, a unimolecular decay (k_i) is present which becomes more invasive as the substrate concentration drops and competition from productive S oxidation decreases. Secondly, a bimolecular decay (k_{2i}) in which one Ac attacks another Ac or Rc is present and also competes with substrate oxidation. This process can be reduced to a negligible level by using very low TAML concentrations (below 10^{-6} M) [13]. At the nM catalyst concentrations usually employed in TAML processes, we have found these bimolecular decay reactions of Ac to be inconsequential [13].

Thus, the operational stability of TAML activators is usually determined principally by the unimolecular suicidal inactivation pathway associated with k_i. If design strategies can be implemented to further reduce k_i without interfering unduly with the positive reactivity features, the technical performance of TAML catalysts will again improve and could take another quantum leap. The core objective is to maximize both the rate of catalysis, usually determined by k_I, and the oxidizing potency of the reactive forms, that correlates with k_{II}, while minimizing the degradation, as determined effectively by k_i. It follows that a simple method for assessing k_i would provide a useful tool for advancing iterative design and would be all the more beneficial to design if it also yielded the other key rate constants controlling the catalytic performance.

For some time, it has been possible to determine k_i values for TAML activators, but the existing approach is viable only under rarified conditions [13]. The rate expression for oxidation of the targeted substrate (S) in the hypothetical absence of catalyst inactivation steps (encompassed by square brackets in Scheme 2 and measured experimentally by monitoring the initial rate of substrate oxidation v) is given by Eq. (1).

$$v = \frac{k_I k_{II}[H_2O_2][S][Fe^{III}]}{k_{-I} + k_I[H_2O_2] + k_{II}[S]} \tag{1}$$

If $k_I[H_2O_2] \gg k_{II}[S]$ and k_{-I} is negligible, Eq. (1) becomes $-d[S]/dt = k_{II}[S][Fe^{III}]$. Under such conditions, the restricted scenario depicted in the dashed box of Scheme 2 is realized. This scenario can be forced experimentally by appropriate selections of the identity and concentration of S, the concentration of H_2O_2 (oxidant), and the reaction

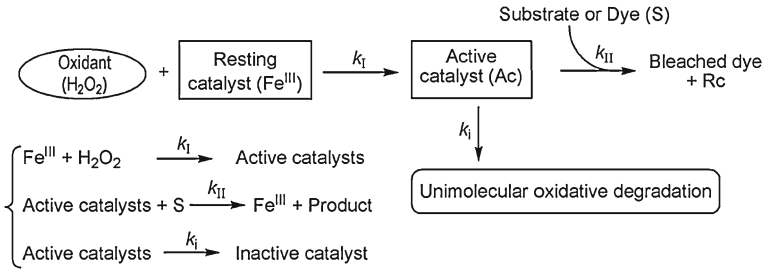

Scheme 3 A sequence of events involving TAML activators analyzed in this work and the corresponding elementary chemical steps used in the mathematical analysis

pH [13]. If one follows the consumption of S experimentally under conditions set such that catalyst degradation terminates the cycle at S_∞, when $t \to \infty$, the variation of S with time t is described by Eq. (2). This relationship allows for the calculation of k_{II} and k_i from a plot of $\ln(\ln([S]/S_\infty))$ versus t [13].

$$\ln\left(\ln\frac{[S]}{S_\infty}\right) = \ln\left(\frac{k_{II}}{k_i}\left[Fe^{III}\right]\right) - k_i t \tag{2}$$

This model and approach has worked well for finding k_{II} and k_i for all first generation (Scheme 1) TAML activators under the restricted conditions of slow reacting substrates, high concentrations of H_2O_2, and high pH [13]. However, Eq. 2 cannot be used when $k_I[H_2O_2] \leq k_{II}[S]$ and TAML activators commonly operate within this regime [10]. As a result, we have not had the ability to evaluate k_{II} while following a wide range of substrate oxidations under diverse conditions. The method is also blind to the rate constant k_I which quantifies a critical step in the catalytic cycle (although k_I has been found by other methods). The "boxed scenario" in Scheme 2 is thus insufficiently general for use in most applications and incapable of providing the rate constant k_I. Therefore, catalyst activation described by k_I was added to give a more complete model requiring new experimental approaches and mathematical formulation and interpretation.

In what follows, the sequence of events shown in Scheme 3 has been analyzed both chemically and mathematically. The rate constant k_{-I} is assumed to be negligible [14,15]. The nonlinear conservation laws inherent to the model have been found and perturbation theory has been applied to derive a first order approximation of the solution for S, Ac, and Rc as functions of time [16]. The result is a formulation of a universal methodology for estimation of the rate constants k_I, k_{II} and k_i from experimentally obtained [S] versus t data which has been employed to parameterize the key rate constants for the new second generation TAML activator **2** (Scheme 1) the synthesis and characterization of which are also described. As a check on the validity of the approach, the rate constants so-obtained have then been compared to those measured using the standard tools of chemical kinetics.

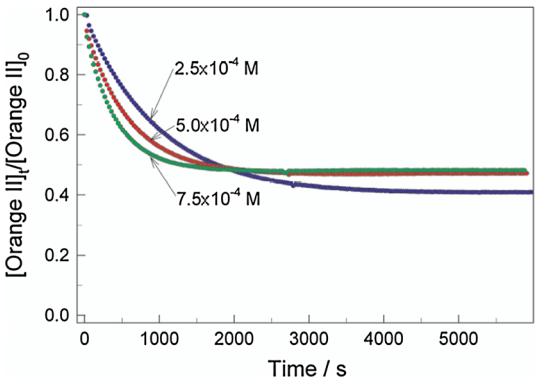

Fig. 1 Incomplete bleaching of Orange II (2.5×10^{-5} M) by H_2O_2 ($2.5 - 7.5 \times 10^{-4}$ M) catalyzed by **2** (1×10^{-7} M) at pH 7 in 0.01 M phosphate buffer at 25 °C

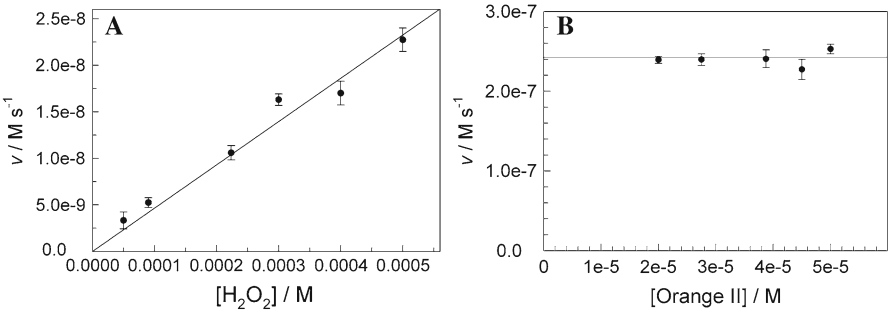

Fig. 2 Initial rates of decolorizing of Orange II by H_2O_2 catalyzed by **2** (1×10^{-7} M) as a function of H_2O_2 (**a**, [Orange II] 4.5×10^{-5} M) and Orange II (**b**, [H_2O_2] 5×10^{-4} M) concentrations at pH 7 0.01 M phosphate) and 25 °C (**a**, **b**)

2.2 General observations

Kinetic traces of incomplete oxidative bleaching of Orange II by H_2O_2 in the presence of the TAML activator **2** at neutral pH when $k_I[H_2O_2] < k_{II}[S]$ are displayed in Fig. 1. Under these conditions the initial rate of oxidative Orange II bleaching is described by the relation $v = k_I[H_2O_2][Fe^{III}]$ (Fig. 2a) and is independent of the amount of dye present (Fig. 2b). Oxidation occurs outside of the kinetic regime that leads to Eq. 2 (the "boxed scenario"). As a result existing approaches cannot be applied. Below is an attempt to resolve this more common case through collaboration between chemical and mathematical teams.

3 Mathematical approach proposed

3.1 Non linear conservation law

The reaction mechanism shown in Scheme 3 transforms into a set of Eqs. (3–5).

$$\frac{dx}{dt} = -k_I^* x + k_{II} y\,[S] \tag{3}$$

$$\frac{dy}{dt} = k_{\mathrm{I}}^{*}x - k_{\mathrm{II}}y\,[\mathrm{S}] - k_{\mathrm{i}}y \tag{4}$$

$$\frac{d\,[\mathrm{S}]}{dt} = -k_{\mathrm{II}}y\,[\mathrm{S}] \tag{5}$$

Here x, y, and [S] are the current concentrations of the Rc [Fe^{III}], Ac, and the Orange II dye, respectively, and $k_{\mathrm{I}}^{*} = k_{\mathrm{I}}[H_2O_2]$ as the concentration of H_2O_2 is assumed to be constant because $[H_2O_2] \gg [\mathrm{S}]$ such that its consumption can be neglected. By using UV-vis spectroscopy, the concentration of Orange II can be easily and accurately measured as a function of time for bleaching curves measured at different peroxide concentrations and therefore it is an observable parameter. The system satisfies the following boundary conditions: $x(0) = x_0$, $y(0) = 0$, $[\mathrm{S}]_0 = \mathrm{S}_0$ and $x_\infty = 0$, $y_\infty = 0$, $[\mathrm{S}]_\infty = \mathrm{S}_\infty$ because all forms of the catalyst eventually vanish. Simple algebraic operations lead to a nonlinear conservation law, of which Eq. (6) is the differential form.

$$\frac{d}{dt}\left(x + y - \frac{k_{\mathrm{i}}}{k_{\mathrm{II}}}\ln[\mathrm{S}]\right) = 0 \tag{6}$$

Integration of Eq. (6) taking into account the initial conditions affords Eq. (7).

$$x = \frac{k_{\mathrm{i}}}{k_{\mathrm{II}}}\ln\left(\frac{[\mathrm{S}]}{\mathrm{S}_0}\right) - y + x_0 \tag{7}$$

Equation (7) allows one to reduce the dimensions of the problem, gives a nonlinear conservation law for this system that can be employed to estimate the rate constants, and as $t \to \infty$ it becomes Eq. (8).

$$\ln\frac{\mathrm{S}_0}{\mathrm{S}_\infty} = \frac{k_{\mathrm{II}}}{k_{\mathrm{i}}}x_0 \tag{8}$$

If $R = \ln\left(\frac{\mathrm{S}_0}{\mathrm{S}_\infty}\right)$ Eq. (8) becomes Eq. (9).

$$k_{\mathrm{II}} = \frac{R}{x_0}k_{\mathrm{i}} \tag{9}$$

This conclusion is identical to that previously reached for the "boxed scenario" in Scheme 1, i.e. when $k_{\mathrm{I}}[H_2O_2] < k_{\mathrm{II}}[\mathrm{S}]$ [9]. Here we have shown that this important relation holds regardless of the relative values of $k_{\mathrm{I}}[H_2O_2]$ and $k_{\mathrm{II}}[\mathrm{S}]$.

3.2 Perturbation solution

Nondimensional concentrations will further be used as $y = x_0\bar{y}$, $x = x_0\bar{x}$, and $[\mathrm{S}] = \mathrm{S}_0[\bar{\mathrm{S}}]$ because the initial concentrations of all the participants are known. An appropriate time scaling is then provided by $t = t_{\mathrm{c}}\tau$ with $t_{\mathrm{c}} = 1/x_0k_{\mathrm{II}}$. Using the conservation law [Eq. (7)] together with the scaling laws, the system of Eqs. (3–5) simplifies to:

$$\frac{d\left[\bar{\mathrm{S}}\right]}{d\tau} = -\bar{y}\left[\bar{\mathrm{S}}\right] \tag{10}$$

$$\frac{\epsilon d\bar{y}}{d\tau} = \beta \ln\left[\bar{\mathrm{S}}\right] - \bar{y}\left(\left[\bar{\mathrm{S}}\right] + \alpha\right) + \zeta \tag{11}$$

where

$$\beta = \frac{k_{\mathrm{I}}^* k_{\mathrm{i}}}{k_{\mathrm{II}}^2 \mathrm{S}_0 x_0}, \alpha = \frac{k_{\mathrm{I}}^* + k_{\mathrm{i}}}{k_{\mathrm{II}} \mathrm{S}_0}, \zeta = \frac{k_{\mathrm{I}}^*}{k_{\mathrm{II}} \mathrm{S}_0}, \epsilon = \frac{x_0}{\mathrm{S}_0} \tag{12}$$

The experimental conditions used in this study imply that ϵ is ca. 10^{-3}. This suggests that a boundary layer exists which separates fast and slow dynamics in the model. Thus, it is appropriate to apply the tools of perturbation theory to this situation [5,16]. The perturbation argument leading to approximate solutions for changes of S concentrations with time both inside and outside the boundary layer of width ϵ can be derived, which can then be assembled into a composite solution through a matching procedure. Outside the boundary layer (in the outer region), regular asymptotic expansions with respect to ϵ in the form of $\bar{y} = \bar{y}_0 + \epsilon\bar{y}_1 \ldots$ and $[\bar{\mathrm{S}}] = \bar{S}_0 + \epsilon\bar{S}_1 \ldots$ have been used for the Ac and the substrate, respectively. A first order approximation then leads to:

$$\frac{d\bar{S}_0}{d\tau} = -\bar{y}\bar{\mathrm{S}}_0 \tag{13}$$

$$0 = \beta \ln\bar{\mathrm{S}}_0 - \bar{y}_0\left(\bar{\mathrm{S}}_0 + \alpha\right) + \zeta \tag{14}$$

This system can be interpreted as a quasi-state approximation commonly used in kinetic modeling [6,17]. In order to derive an analytical solution, an approximation of the form $\bar{\mathrm{S}}_0 + \alpha \sim A(\alpha+1)$ is introduced, with A being a constant independent of k_{I}, k_{II}, and k_{i}. This approximation holds for the outer layer, where S_0 changes only slightly. This allows one to obtain the following representation for the substrate change in the outer region:

$$\bar{\mathrm{S}}_0 = e^{-\frac{\zeta}{\beta}} e^{\frac{C}{\beta}} \mathrm{e}^{\left(-\frac{\beta}{A(\alpha+1)}\tau\right)} \tag{15}$$

Here C is an integration constant to be determined. Note that $\zeta/\beta = R$, so Eq. (15) can be further simplified as:

$$\bar{\mathrm{S}}_0 = \frac{\mathrm{S}_\infty}{\mathrm{S}_0} e^{\frac{C}{\beta}} e^{\left(-\frac{\beta}{A(\alpha+1)}\tau\right)} \tag{16}$$

By plugging (16) into (14), one obtains the corresponding representation of the Ac behavior in the outer region:

$$\bar{Y} = \bar{y}_0 = \frac{C}{A(\alpha+1)} e^{\left(-\frac{\beta}{A(\alpha+1)t_C}t\right)} \tag{17}$$

These are the explicit outer region solutions for the concentrations of the Ac [Eq. (17)] and of the substrate [(S)] [Eq. (16)]. The outer solution is denoted by $\bar{Y}$ to distinguish it from the inner solution. Note that $\bar{\mathrm{S}}_0 \to \mathrm{S}_\infty/\mathrm{S}_0$ and $\bar{y}_0 \to 0$ as $\tau \to \infty$, as expected.

To approximate the solution in the inner region, a singular perturbation expansion to zoom into the boundary layer was performed. If τ is scaled by $\tau = \bar{\tau}\epsilon$, the first order approximation generates:

$$\frac{d\bar{S}_0}{d\bar{\tau}} = 0 \tag{18}$$

$$\frac{d\bar{y}_0}{d\bar{\tau}} = \beta \ln \bar{S}_0 - \bar{y}_0 \left(\alpha + \bar{S}_0\right) + \zeta \tag{19}$$

which implies

$$\left[\bar{S}\right] = \bar{S}_0 = 1 \tag{20}$$

$$\bar{y} = \bar{y}_0 = \frac{\zeta}{\alpha + 1}\left(1 - e^{-\frac{(\alpha+1)}{t_c \epsilon}t}\right) \tag{21}$$

These inner solutions for [S] and the Ac are denoted as $[\bar{S}]$ and $\bar{y}$, respectively. To match the values of $\bar{y}$ and $\bar{Y}$ at the boundary layer, the following condition should be imposed:

$$\lim_{t \to 0} \bar{Y} = \lim_{t \to \infty} \bar{y}$$

This is necessary because the outer solution must match the inner solution as time approaches zero. In the same fashion, the inner solution must match the outer solution as time approaches infinity. By applying the previous condition to the Ac and S, one can see that this condition is equivalent to: $R = AR,\ C = \zeta$. We conclude that $A = 1$ and set the value of the integration constant to $C = \zeta$. After matching the two pieces of the solution, the following composite solution is obtained:

$$\frac{y}{x_0} = \frac{\zeta}{\alpha + 1}\left(e^{\frac{-\beta}{(\alpha+1)t_c}t} - e^{\frac{-(\alpha+1)}{\epsilon t_c}t}\right) \tag{22}$$

$$\frac{[S]}{S_0} = \frac{S_\infty}{S_0} e^{Re^{\frac{-\beta}{(\alpha+1)t_c}t}} \tag{23}$$

Equations (22)–(23) are the final closed form asymptotic solutions for the Ac and S which will be used hereafter. The concentration of S as in Eq. (23) satisfies Eq. (24).

$$\ln\left(\ln\frac{[S]}{S_\infty}\right) = \ln R - M_1 t \tag{24}$$

where

$$M_1 = \frac{\beta}{(\alpha + 1)\, t_c} \tag{25}$$

Equation (24) is the unrestricted analogue of Eq. (2). A double logarithmic plot of $[S]/S_\infty$ versus time t should be a linear function of time with the intercept and slope of $\ln R$ and $-M_1$, respectively ($M_1 > 0$). Expanding the expression for M_1 using Eq. (12), one gets:

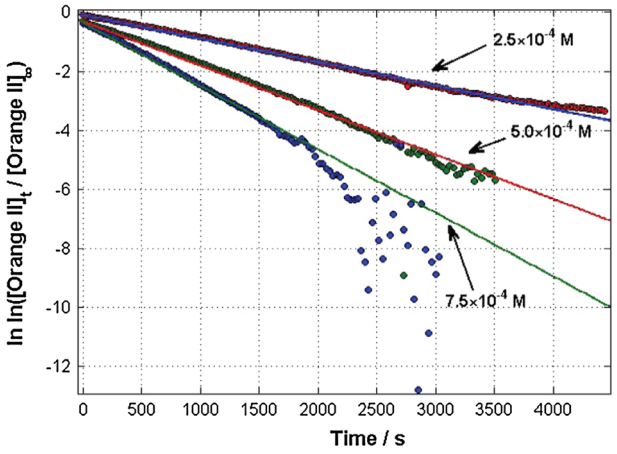

Fig. 3 Linear least squares fitting of the experimental data in Fig. 1 to Eq. (24)

$$M_1 = \frac{k_{\mathrm{I}}\,[\mathrm{H_2O_2}]\,k_{\mathrm{i}}}{k_{\mathrm{I}}\,[\mathrm{H_2O_2}] + k_{\mathrm{i}} + k_{\mathrm{II}}\mathrm{S}_0} \tag{26}$$

It is worth noting that when $t \to \infty$, Eq. (24) agrees with the definition $R = \ln(\mathrm{S}_0/\mathrm{S}_\infty)$, and Eq. (26) converts to k_{i} when $k_{\mathrm{I}}[\mathrm{H_2O_2}] \gg k_{\mathrm{i}} + k_{\mathrm{II}}[\mathrm{S}]$ which agrees with the earlier approach [13]. Results of a linear least squares fitting of the experimental data for three different concentrations of $\mathrm{H_2O_2}$ are shown in Fig. 3. A good straight-line approximation is observed for 5–10 half-lives. Small deviations observed at the highest $\mathrm{H_2O_2}$ concentrations are negligible due to the fact that no bleaching actually occurs after 2,000 s.

3.3 Estimation of the rate constants

The solution given by Eq. (23) was applied to solve the inverse problem, i.e. to estimate the rate constants k_{I}, k_{II} and k_{i} from the experimental data given in Fig. 1. The slopes of the straight lines in Fig. 3 obtained using Equation (24) depend on $\mathrm{H_2O_2}$ concentration. From Eqs. (9) and (26) it comes

$$k_{\mathrm{i}} = \frac{M_1 x_0 k_{\mathrm{I}}^*}{x_0 k_{\mathrm{I}}^* - x_0 M_1 - M_1 \mathrm{S}_0 R} \tag{27}$$

Here M_1 denotes the slope obtained from the fit, and R is the same constant as appears in Eq. (9). Equation (26) can be presented as

$$\frac{1}{M_1} = \frac{1}{k_{\mathrm{i}}} + M_2 \frac{1}{[\mathrm{H_2O_2}]} \tag{28}$$

$$M_2 = \frac{k_{\mathrm{i}} + k_{\mathrm{II}}\mathrm{S}_0}{k_{\mathrm{I}} k_{\mathrm{i}}} \tag{29}$$

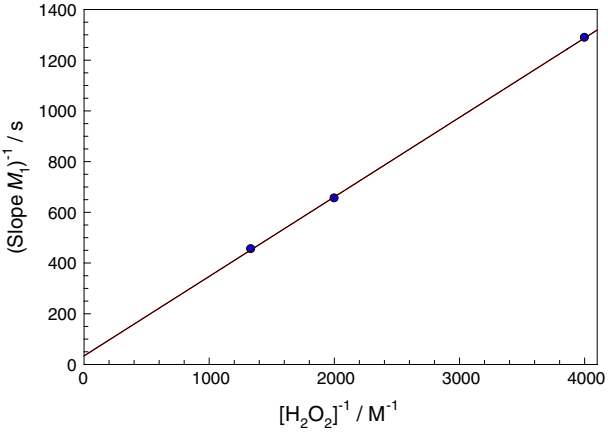

Fig. 4 Double reciprocal plot of the slopes M_1 versus peroxide concentrations. The linear fit results in a slope of $M_2 = 0.3123$

The inverse of the slopes M_1 vary linearly with inverse peroxide concentrations [Eq. (28)] and the slope and the intercept equal M_2 and k_i^{-1}, respectively (Fig. 4).

Finally, combining Eqs. (9) and (29) gives the expression for the rate constant k_I.

$$k_I = \frac{x_0 + S_0 R}{x_0 M_2} \tag{30}$$

Combination of Eqs. (30) and (27) gives the expression for k_i.

$$k_i = \frac{M_1 [H_2O_2]}{[H_2O_2] - M_1 M_2} \tag{31}$$

Equations (9), (30), and (31) are the key equations for computing the rate constants. A routine has been developed for the determination of k_I, k_{II}, and k_i.

Mathematical algorithm (MA) for estimating the rate constants:

GIVEN: [S] versus t data measured at several different $[H_2O_2]$ with the same $[S]_0$ and x_0 as shown in Fig. 1.
PROCEDURE:

1. For each $[H_2O_2]$ data set, one computes the corresponding value of $R = \ln(S_0/S_\infty)$ using the best approximation of S_∞ available.
2. For each $[H_2O_2]$ data set, one fits the data to Eq. (24) to get M_1.
3. Using M_1 obtained in Step 2, one fits M_1^{-1} versus $[H_2O_2]^{-1}$ to Eq. (28) to get M_2.
4. One calculates k_I from Eq. (30) for each data set.
5. One calculates k_i from Eq. (31) for each data set.
6. One uses k_i obtained in Step 5 to calculate k_{II} using Equation (9) for each data set.

The rate constants k_I, k_{II}, and k_i can be calculated from kinetic data such as are shown in Fig. 1 for the oxidation of any substrate by any peroxide provided the kinetic

data are collected at different concentrations of peroxide. Estimating M_2 by the slope is rather accurate even for a small number of data points (experimental data sets) due to the inherently linear nature of the dependence of M_1^{-1} on $[H_2O_2]^{-1}$, while the accuracy of M_1^{-1} estimation is reliant upon the quality of experimental observations for 5–10 half-lives in each of the data sets. The rate constants calculated by the MA for the new dicyano-substituted iron(III)-containing TAML activator **2** are shown in Table 1.

The new method provides explicit equations for the current concentrations of Ac, Rc, and substrate as a function of time without a priori knowledge of the rate constants. In fact, Eqs. (3–5) afford

$$[\mathrm{S}] = \mathrm{S}_\infty e^{Re^{-M_1 t}} \tag{32}$$

$$y = \frac{x_0\,\zeta}{\alpha+1}\left(e^{-M_1 t} - e^{-(k_\mathrm{I}^* + k_\mathrm{i} + k_\mathrm{II}\mathrm{S}_0)t}\right) \tag{33}$$

$$x = \frac{x_0}{R}\ln\left(\frac{[\mathrm{S}]}{\mathrm{S}_0}\right) - y + x_0 \tag{34}$$

where

$$R = \frac{\zeta}{\beta},\ M_1 = \frac{\beta}{(\alpha+1)\,t_\mathrm{c}},\ t_\mathrm{c} = \frac{1}{x_0 k_\mathrm{II}},\ \beta = \frac{k_\mathrm{I}^* k_\mathrm{i}}{k_\mathrm{II}^2 \mathrm{S}_0 x_0},\ \alpha = \frac{k_\mathrm{I}^* + k_\mathrm{i}}{k_\mathrm{II}\mathrm{S}_0},\ \zeta = \frac{k_\mathrm{I}^*}{k_\mathrm{II}\mathrm{S}_0} \tag{35}$$

and the accuracy is on the order of ϵ, where

$$\epsilon = \frac{x_0}{S_0} \tag{36}$$

4 Verification of the new mathematical algorithm (MA)

To verify the rate constants obtained by the MA, one has to validate the closed-form solutions to the original system of stiff nonlinear differential equation against available data. Figure 5a compares the solution obtained by the MA with the experimentally measured decrease of [Orange II]. It is easy to see that the two curves match almost perfectly. For additional benchmarking, in Fig. 6b the solutions given in Eqs. (32–33) are also compared to the numerical solutions of the original nonlinear system (3–5). Numerical approximations are obtained by a commonly used MATLAB implementation ode23s of the stiff ODE solver based on a modified second order Rosenbrock formula (as described elsewhere [18]). While the MA solution is reasonably close to that obtained by ode23s, the smoother (and hence more chemically plausible) behavior of the solution provided by MA as visible in the insert of Fig. 6b reflects a better approximation around the boundary layer.

Since estimation of k_II cannot be performed by a simple routine under conditions where $k_\mathrm{I}[H_2O_2] \leq k_\mathrm{II}[S]$ and particularly when $k_\mathrm{I}[H_2O_2] \ll k_\mathrm{II}[S]$, i.e. when the reaction rate does not depend on [S] [19], the terms $k_\mathrm{I}[H_2O_2]$ and $k_\mathrm{II}[\mathrm{S}]$ are made comparable by choosing appropriate concentrations of H_2O_2 and S. As seen in the

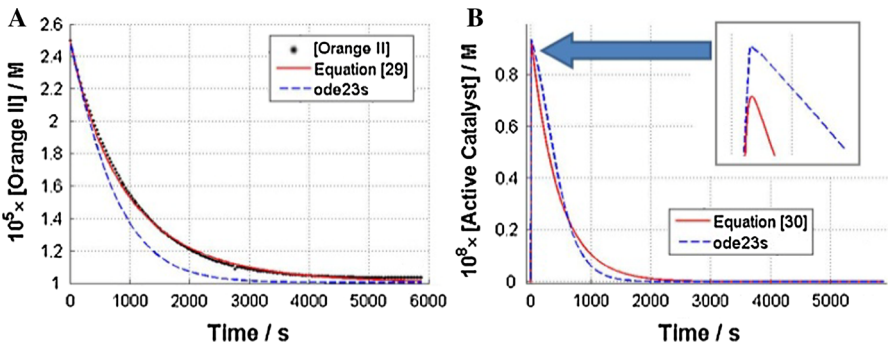

Fig. 5 Comparison of the new approximation (32,33) with experimentally measured Orange II data collected at $[H_2O_2] = 2.5 \times 10^{-4}$, $[\text{Orange II}]_0 = 2.5 \times 10^{-5}$ in 0.01 M phosphate buffer at pH 7 and the solutions obtained by the ode23s stiff ODE solver

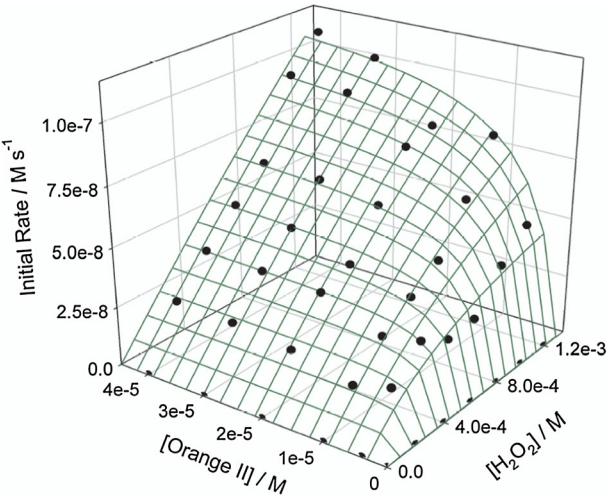

Fig. 6 3D plot for the initial rate of the Orange II bleaching by H_2O_2 catalyzed by 2 (2×10^{-7}M) as a function of Orange II and H_2O_2 concentrations at pH 7 (0.01 M phosphate) and 25 °C. Each data point is a mean value of four determinations

3D plot in Fig. 6, concentrations at which the reaction rate depends on the amount of Orange II are rather limited. In most cases the reaction rate is independent of [Orange II] and is a linear function of $[H_2O_2]$ as it is seen in Fig. 2. All data points in Fig. 6, which are mean values of four determinations, were fitted to Eq. (1) assuming $k_{-\text{I}} \approx 0$ and the rate constants k_{I} and k_{II} obtained are shown in Table 1. The value of k_{I} calculated from the data in Fig. 2a agrees well with k_{I} calculated from the 3D plot. The rate constants k_{i} were then estimated using Eq. (9).

The rate constants obtained by the MA and the standard chemical routine agree. Importantly, the values are close for all three rate constants k_{I}, k_{II} and k_{i} though significantly less experimental data are needed for the MA routine compared with the standard chemical approach which requires a 3D surface such as that in Fig. 6.

Table 1 Rate constants k_I, k_{II} (both in $M^{-1}s^{-1}$) and k_i (s^{-1}) obtained using the MA and standard chemical routines at pH 7 and 25°C

$10^4 \times [H_2O_2]$/M	MA			Chemical Routine		
	k_I	$10^{-5} \times k_{II}$	$10^2 \times k_i$	k_I	$10^{-5} \times k_{II}$	$10^2 \times k_i$
2.5	733 ± 15	2.2 ± 0.5	2.4 ± 0.5			1.3 ± 0.2
5.0	593 ± 15	2.0 ± 0.3	2.7 ± 0.3	465 ± 20	1.2 ± 0.2	1.6 ± 0.3
7.5	564 ± 15	1.6 ± 0.2	2.3 ± 0.2			1.6 ± 0.3

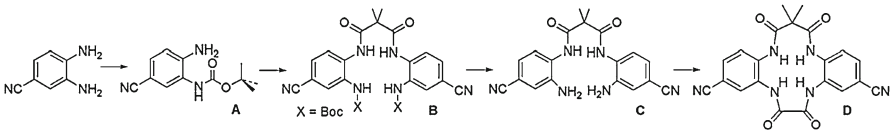

Fig. 7 Synthesis of **2**

5 Conclusion

A new methodology for modeling chemical catalytic oxidation systems which operate via the mechanism shown in Scheme 3 is described. A simple routine for estimating rate constants regardless of the relative values of k_I, k_{II} and k_i is demonstrated. The Mathematical Algorithm (MA) is consistent with the method developed previously, which is applicable only when $k_I[H_2O_2] \gg k_{II}[S]$ [13]. The MA facilitates the calculation of k_i under all conditions using Eq. (9) provided k_{II} is known. MA affords the rate constants and the time-dependent conversion of the substrate and all forms of the catalyst. The easy-to-use Eqs. (24) and (28) eliminate the need to collect large data sets that are required if the traditional chemical kinetics approach is used. Additionally, the approach is transferable to other oxidation mechanisms. Current work is focused on performing systematic analyses of additional systems of this type to further understand how catalyst design impacts operational stability.

6 Experimental section

General details Spectrophotometric measurements were carries out on Hewlett-Packard Diode Array spectrophotometers (models 8452A and 8453) equipped with a thermostatted cell holder and automatic 8-cell positioner. ^{1}H NMR data were collected at 300 K with a Bruker Avance 300 operating at 300 MHz using DMSO-d_6 with chemical shifts referenced to the residual proton DMSO peak at $\delta = 2.5$; J values are in Hz. Elemental analyses were performed by Midwest Microlab, Indianapolis, IN. Electrospray ionization mass spectra (ESI-MS) were obtained using a Finnigan MAT SSQ700 mass spectrometer with an Analytical of Branford electrospray ionization interface. THF was freshly distilled from Na/ benzophenone ketyl under an argon atmosphere. All reagents and solvents were of ACS reagent grade and were used without further purification.

Synthesis of **2***, as shown in Figure* 7: 3,4-Diaminobenzonitrile was protected by di- tert-butyl dicarbonate (Boc_2O) in THF as previously described [20]. *tert*-Butyl 2-amino-4-cyanophenylcarbamate (**A**) was purified by SiO_2 flash chromatography on 60 mesh gel pretreated with NEt_3 (gradient elution, hexanes: EtOAc 3:1 to EtOAc) and isolated as a pale orange solid (1.961 g, 56 %). ^{1}H NMR: 1.46 (s, 9H, CH_3), 5.88 (s, 2H, NH_2), 6.72 (d, J 8.4, 1H, phenyl), 7.21 (d, J 8.3, 2.1; 1H, phenyl), 7.61 (d, *J* 2.1, 1H, phenyl) 8.43 (s, 1H, NHCO). Dimethylmalonyl chloride (3.44 mmol, 582 mg) in THF (23 mL) was added dropwise to a stirred solution of **A** (6.88 mmol, 1.605 g) and pyridine (8.60 mmol, 680 mg) in THF (103 mL) under argon at 22 °C.The reaction mixture was filtered after 24 h and concentrated in vacuo to yield **B**. ^{1}H NMR : 1.41 (s, 18H, methyl), 1.56 (s, 6H, methyl), 7.58 (dd, *J* 2.1, 8.4, 2H, phenyl), 7.79 (d, *J* 8.4, 2H, phenyl), 7.87 (d, *J* 2.1, 2H), 8.93 (s, 2H, BocNHCO), 9.54 (s, 2H, malonylNH CO).HCl (12.1N, 2.3 mL) was added to a stirred solution of **B** (0.088 mmol, 50 mg) in EtOAc (16 mL) under argon at 22 °C. Visible evolution of gas stopped after 15 min and the reaction was quenched by 1 M $NaHCO_3$ at 0 °C. The organic layer was separated after 30 min of vigorous stirring and the aqueous phase was extracted with EtOAc (3 × 20 mL). The combined organic layers were dried over Na_2SO_4, filtered, and concentrated in vacuo to yield **C** as a white solid (28 mg, 86 %). ^{1}H NMR : 1.56 (s, 6H, CH_3), 5.34 (s, 4H, NH_2), 6.95 (dd, *J* 8.2, 2.1, 2H, phenyl), 7.05 (d, *J* 2.1, 2H, phenyl), 7.22 (d, *J* 8.2, 2H, phenyl), 9.24 (s, 1H, NHCO). A solution of oxalyl chloride (0.138 mmol, 0.07 mL, 2.0 M in CH_2Cl_2) in THF (14 mL) was added dropwise to a stirred solution of **C** (0.138 mmol, 50 mg) and NEt_3 (0.276 mmol, 39 μL) in a round bottom flask under argon at 22 °C. The crude mixture was filtered after 24 h through a medium porosity glass frit and rinsed five times with deionized water to yield **D** as a white solid (54 mg, 94 %): ^{1}H NMR : 1.54 (s, 6H, CH_3), 7.62 (d, *J* 8.1, 2H, phenyl), 7.78 (dd, *J* 1.8, *J* 8.1, 2H, phenyl), 7.96 (d, *J* 1.8Hz, 2H, phenyl), 10.03 (s, 1H,oxalyl NHCO), 10.19 (s, 1H, malonyl NHCO). Anal. Calcd (found) for $C_{21}H_{16}N_6O_4 \cdot 1.5H_2O$: C, 56.88 (56.72); H, 4.32 (4.25); N, 18.95 (17.72). A solution of $LiN(Si(CH_3)_3)_2$ (0.53 mmol, 0.53 mL, 1.0 M in hexanes) in THF (0.64 mL) was added to a rapidly stirred suspension of **D** (0.120 mmol, 50 mg) in THF (15 mL) at 22 °C under argon resulting in a light-orange solution. A solution of $FeCl_3$ (0.132 mmol, 21.4 mg) in THF (11.36 mL) was introduced after 10 min to afford a dark brown solution exposed to the air after 15 min and allowed to stir for 30 min. It was concentrated in vacuo to give a dark brown solid to which HPLC grade water (7 mL) was added. The solution was filtered, concentrated in vacuo, and the residue was purified by reverse phase flash chromatography on C18 silica gel (gradient elution HPLC grade H_2O to 10:1 HPLC H_2O: HPLC MeOH) to give **2** (42 mg, 74 %) as a lithium salt. ESI-MS neg. mode: m/z 468.2, Anal. Calcd (found) for $C_{21}H_{12}FeLiN_6O_4 \cdot 3H_2O$: C, 46.09 (45.88); H, 3.68 (3.35); N, 15.36 (13.89).

Kinetic Studies of Bleaching of Orange II by H_2O_2 *catalyzed by* **2** *Stock solutions of* **2** (5×10^{-6} M) and Orange II (4.5×10^{-5} M) were prepared in both HPLC grade methanol and water, respectively. H_2O_2 (2×10^{-2} M) solutions were prepared in 0.01 M phosphate buffer pH 7 and standardized daily by measuring the absorbance at 230 nm (ε 72.8 $M^{-1}cm^{-1}$) [21]. Aliquots of stock solutions of Orange II and **2** were added to a polymethylmethacrylate UV-vis cuvette followed by the 0.01 M pH 7 phosphate buffer

to reach a final volume of 1 mL. The cell holder was thermostatted at 25 °C. Initial rates of Orange II oxidation were calculated using the pH 7 extinction coefficient for Orange II of 18,100 M^{-1} cm^{-1}. Initial rates reported are mean values of at least four determinations. Rate constants k_I and k_{II} were calculated using a Sigma Plot 2010 package (version 12.0).

Acknowledgments The authors are grateful to Dan Anderson, Pak-Wing Fok, Angela Dapolite and Joshua Patent for fruitful discussions and contributions at the early stages of the work. In addition, support is acknowledged of the Heinz Endowments (T.J.C.) and the Institute for Green Science (T.J.C). NMR instrumentation at CMU was partially supported by National Science Foundation (CHE-0130903 and CHE-1039870). M.E. acknowledges National Science Foundation support under DMS-202340.

References

1. H.B. Dunford, *Heme Peroxidases* (Wiley-VCH, New York, 1999)
2. T.J. Collins, S.W. Gordon-Wylie et al., in P.T. Anastas, T.C Williamson, ed. by *Green Chemistry* (Oxford University Press, Oxford, 1998), pp. 46–71
3. T.J. Collins, TAML oxidant activators: a new approach to the activation of hydrogen peroxide for environmentally significant problems. Acc. Chem. Res. **35**, 782–790 (2002)
4. T.J. Collins, Designing ligands for oxidizing complexes. Acc. Chem. Res. **27**, 279–285 (1994)
5. T. Turanyi, A.S. Tomlin, M.J. Pilling, On the error of the quasi-steady-state approximation. J. Phys. Chem. **97**, 163–172 (1993)
6. W. Richardson, L. Volk, K.H. Lau, S.H. Lin, H. Eyring, Application of the singular perturbation method to reaction kinetics. Proc. Natl. Acad. Sci. USA **70**, 1588–1592 (1973)
7. M. Lazman, G. Yablonsky, in *Advances in Chemical Engineering: Mathematics and Chemical Engineering and Kinetics*. Vol. 34 (Academic Press, 2008)
8. N.S. Shuman, T.M. Miller, A.A. Viggiano, J. Troe, Electron attachment to CF3 and CF3Br at temperatures up to 890 K: experimental test of the kinetic modeling approach. J. Chem. Phys. **138**, 204316 (2013)
9. C. Jiménez-Borja, B. Delgado, F. Dorado, J.L. Valverde, Experimental data and kinetic modeling of the catalytic and electrochemically promoted CH_4 oxidation over Pd catalyst-electrodes. Chem. Eng. J. **225**, 315–322 (2013)
10. A.D. Ryabov, T.J. Collins, Mechanistic considerations on the reactivity of green FeIII-TAML activators of peroxides. Adv. Inorg. Chem. **61**, 471–521 (2009)
11. A. Ghosh, A.D. Ryabov, S.M. Mayer, D.C. Horner, D.E. Prasuhn Jr., S. Sen Gupta, L. Vuocolo, C. Culver, M.P. Hendrich, C.E.F. Rickard et al., Understanding the mechanism of H^+-induced demetalation as a design strategy for robust iron(III) peroxide-activating catalysts. J. Am. Chem. Soc. **125**, 12378–12379 (2003)
12. V. Polshin, D.-L. Popescu, A. Fischer, A. Chanda, D.C. Horner, E.S. Beach, J. Henry, Y.-L. Qian, C.P. Horwitz, G. Lente et al., Attaining control by design over the hydrolytic stability of Fe-TAML oxidation catalysts. J. Am. Chem. Soc. **130**, 4497–4506 (2008)
13. A. Chanda, A.D. Ryabov, S. Mondal, L. Alexandrova, A. Ghosh, Y. Hangun-Balkir, C.P. Horwitz, T.J. Collins, The activity-stability parameterization of homogeneous green oxidation catalysts. Chem. Eur. J. **12**, 9336–9345 (2006)
14. N. Chahbane, D.-L. Popescu, D.A. Mitchell, A. Chanda, D. Lenoir, A.D. Ryabov, K.-W. Schramm, T.J. Collins, Fe^{III}-TAML-catalyzed green oxidative degradation of the azo dye orange II by H_2O_2 and organic peroxides: products, toxicity, kinetics, and mechanisms. Green Chem. **9**, 49–57 (2007)
15. D.-L. Popescu, M. Vrabel, A. Brausam, P. Madsen, G. Lente, I. Fabian, A.D. Ryabov, R. van Eldik, T.J. Collins, Thermodynamic, electrochemical, high-pressure kinetic, and mechanistic studies of the formation of Oxo FeIV-TAML species in water. Inorg. Chem. **49**, 11439–11448 (2010)
16. M.H. Holmes, *Introduction to Perturbation Methods* (Springer, New York, 1995)
17. Holmes, M.H. *Introduction to the Foundations of Applied Mathematics* (Springer Texts in Applied Mathematics, 2009)
18. L.F. Shampine, M.W. Reichelt, The MATLAB ODE suite. SIAM J. Sci. Comput. **18**, 1–22 (1997)

19. A. Ghosh, D.A. Mitchell, A. Chanda, A.D. Ryabov, D.L. Popescu, E. Upham, G.J. Collins, T.J. Collins, Catalase-peroxidase activity of iron(III)-TAML activators of hydrogen peroxide. J. Am. Chem. Soc. **130**, 15116–15126 (2008)
20. W.C. Ellis, C.T. Tran, R. Roy, M. Rusten, A. Fischer, A.D. Ryabov, B. Blumberg, T.J. Collins, Designing green oxidation catalysts for purifying environmental waters. J. Am. Chem. Soc. **132**, 9774–9781 (2010)
21. P. George, The chemical nature of the second hydrogen peroxide compound formed by cytochrome c peroxidase and horseradish peroxidase. Biochem. J. **54**, 267–262 (1953)